Characterization of MCM-48 Materials

Kai Schumacher,[†] Peter I. Ravikovitch,[‡] Alexander Du Chesne,[§] Alexander V. Neimark,*[,‡] and Klaus K. Unger[†]

Institut für Anorganische Chemie und Analytische Chemie, Johannes Gutenberg Universität, Duesbergweg 10−14, 55099 Mainz, Germany; TRI/Princeton, 601 Prospect Avenue, Princeton, New Jersey 08542-0625; and Max Planck Institut für Polymerforschung, Ackermannweg 10, 55128 Mainz, Germany

Received December 7, 1999. In Final Form: February 14, 2000

Mesoporous molecular sieves of MCM-48 type were prepared by conventional hydrothermal and novel room temperature syntheses. Scanning electron microscopy (SEM) studies have shown that nonagglomerated uniform spheres of size ca. 0.5 μm were obtained by the room temperature method. Internal pore structure was studied by X-ray diffraction (XRD), transmission electron microscopy (TEM), and high-resolution nitrogen and argon adsorption. Pore size distributions were calculated from low-temperature nitrogen and argon adsorption isotherms by the nonlocal density functional theory (NLDFT) method. A novel approach to calculating the pore wall thickness of MCM-48 from XRD and gas adsorption isotherms was employed. The approach utilizes intrinsic symmetry of MCM-48 pore structure, cubic *Ia*3*d* space group, revealed by XRD and combines the results of the pore size distribution analysis with general geometrical relations between structural parameters of the gyroid minimal surface. The pore wall thickness of MCM-48 calculated from both nitrogen and argon adsorption data was found to be ca. 8−10 Å, in good agreement with the estimates obtained from TEM.

1. Introduction

In 1992, a new family of mesoporous materials, designated as M41S, was introduced by Mobil researchers.[1] M41S materials are formed via liquid-crystal mechanism through mesostructures defined by aggregation of organic template molecules. M41S materials possess well-defined pore structures. The most popular members of this family are MCM-41 and MCM-48. MCM-41 has a hexagonal array of unidirectional pores. MCM-48 has a cubic pore system, which is indexed in the space group *Ia*3*d* (Figure 1). On the basis of X-ray diffraction (XRD) and transmission electron microscopy (TEM) studies, MCM-48 material has been found to possess a bicontinuous structure centered on the gyroid minimal surface[2] that divides available pore space into two nonintersecting subvolumes (Figure 2).[3,4]

In the past few years, much work has been done on MCM-41.[3,5−7] Several synthesis routes have been developed for this material, and extensive sorption studies have been done. Because of its simple structure, MCM-41 has become a model substance for sorption studies.[8−21]

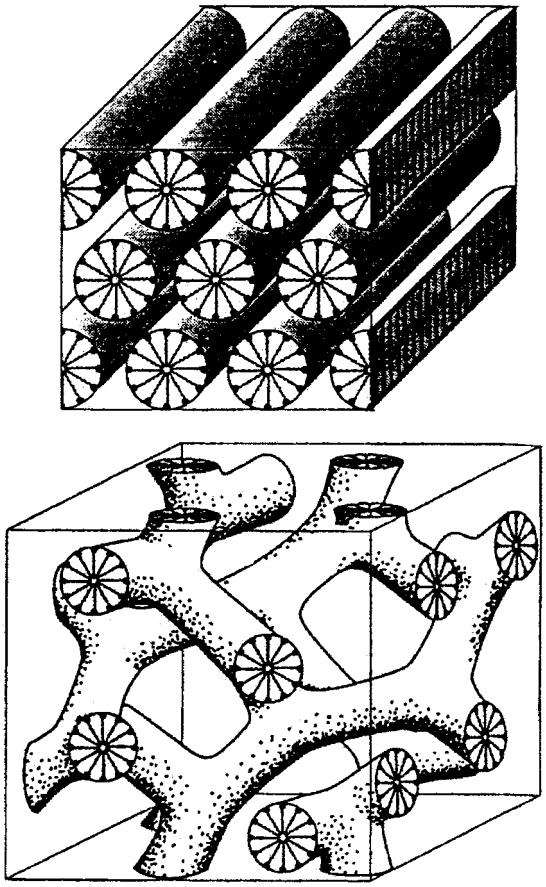

Figure 1. Structure of MCM-41 (top) and MCM-48 (bottom).

Recently, MCM-48 has been attracting the increasing interest of researchers.[3,5,22−29] MCM-48 can be synthesized

* Author for correspondence. E-mail: aneimark@triprinceton.org.
[†] Johannes Gutenberg Universität.
[‡] TRI/Princeton.
[§] Max Planck Institut für Polymerforschung.

(1) (a) Kresge, C. T.; Leonowicz, M. E.; Roth, W. J.; Vartuli, J. C.; Beck, J. S. *Nature* **1992**, *359*, 710. (b) Beck, J. S.; Vartuli, J. C.; Roth, W. J.; Leonowicz, M. E.; Kresge, C. T.; Schmitt, K. D.; Chu, C. T.-W.; Olson, D. H.; Sheppard, E. W.; McCullen, S. B.; Higgins, J. B.; Schlenker, J. L. *J. Am. Chem. Soc.* **1992**, *114*, 10834.

(2) Schoen, A. H. *Infinite Periodic Minimal Surfaces without Intersections;* NASA Technical Note TD-5541, 1970.

(3) Monnier, A.; Schüth, F.; Huo, Q.; Kumar, D.; Margolese, D.; Maxwell, R. S.; Stucky, G. D.; Krishnamurty, M.; Petroff, P.; Firouzi, A.; Janicke, M.; Chmelka, B. F. *Science* **1993**, *261*, 1299.

(4) Alfredsson, V.; Anderson, M. W. *Chem. Mater.* **1996**, *8*, 1141.

(5) Huo, Q.; Margolese, D. I.; Stucky, G. D. *Chem. Mater.* **1996**, *8*, 1147.

(6) Ciesla, U.; Grün, M.; Isajeva, T.; Kurganov, A. A.; Neimark, A. V.; Ravikovitch, P. I.; Schacht, S.; Schüth, F.; Unger, K. K. In *Access in Nanoporous Materials*; Pinnavaia, T. J., Thorpe, M. F., Eds.; Plenum Press: New York, 1995; p 231.

(7) Grün, M.; Unger, K. K.; Matsumoto, A.; Tsutsumi, K. In *Charaterization of Porous Solids IV*; McEnaney, B.; Mays, T. J.; Rouquérol, J.; Rodríguez-Reinoso, F.; Sing, K. S. W.; Unger, K. K., Eds.; The Royal Society of Chemistry: London, 1997; p 81.

(8) Branton, P. J.; Hall, P. G.; Sing, K. S. W.; Reichert, H.; Schüth, F.; Unger, K. K. *J. Chem. Soc. Faraday Trans.* **1994**, *90*, 2965.

10.1021/la991595i CCC: $19.00
Published on Web 04/07/2000

by different ways with highly specific surface area, specific pore volume, and narrow pore size distribution. It shows high thermal stability up to 750 °C. Catalytic properties can be adjusted by incorporation of different metals (e.g., Ti, Nb, Al, V) into the MCM-48 framework.[23−25] Several catalytic applications are described in the literature, e.g., *n*-decane conversion and carbon dioxide reduction.[26,27] The regular pore network of MCM-48, which provides more favorable mass transfer kinetics than the unidirectional pore system of MCM-41, seems to be a promising candidate for applications in catalytic and separation technologies, e.g., supercritical fluid chromatography (SFC).[28]

Approaches to synthesis of MCM-48 differ in the pH of reaction medium, catalyst used, reaction time, and temperature.[1,3,5,22,23] In this paper, we report on XRD, TEM, scanning electron microscopy (SEM), and sorption characterization studies of MCM-48 materials prepared by different synthesis conditions, including a new room temperature synthesis developed earlier.[23] The pore size distributions of MCM-48 are calculated from nitrogen and argon adsorption isotherms by the accurate nonlocal density functional theory (NLDFT) method.[16−18] We are particularly interested in determination of the pore wall thickness in MCM-48. This information cannot be extracted from the XRD data. It was also shown that the simulated TEM images of the gyroid based structures are not very sensitive to the variations in the wall thickness from 3 to 13 Å.[4] In this work, we apply a novel method for calculating the pore wall thickness of MCM-48 by combining sorption and XRD data.[29]

2. Experimental Section

2.1. Sample Preparation. Samples 1 and 2 were synthesized by the conventional hydrothermal pathway similar to the procedure described by Monnier et al.[3] *N*-hexadecyltrimethylammonium bromide was dissolved in deionized water, and sodium hydroxide and TEOS were added. The molar composition of the gel was 1 M TEOS:0.25 M Na_2O:0.65 M $C_{16}H_{33}(CH_3)_3NBr$:0.62 M H_2O. The solution was stirred for about 1 h, charged into a polypropylene bottle, and heated at 383 K for 3 (sample 1) and 10 days (sample 2). The product was filtered, washed with water, and calcined at 823 K for 6 h.

Samples 3−5 were prepared by a room temperature synthesis developed earlier.[23] A 2.6 g aliquot of *N*-hexadecyltrimethylammonium bromide (Aldrich, Steinheim, Germany, 6.6 mmol) was dissolved in 120 g of deionized water and 50 mL of technical ethanol (Merck KGaA, Darmstadt, Germany, 0.87 mol), and 12 mL of aqueous ammonia (Merck KGaA, Darmstadt, Germany, 32 wt %, 0.20 mol) was added to the surfactant solution. The solution was stirred for 10 min (450 rpm), and 3.4 g of TEOS (Aldrich, Steinheim, Germany, 98%, 16 mmol) was added at one time. The molar composition of the gel was 1 M TEOS:12.5 M NH_3:54 M EtOH:0.4 M template:417 M H_2O.

After being stirred for 10 (sample 3), 3.5 (sample 4), and 24 h (sample 5) at room temperature, the resulting solid was recovered by filtration, washed with distilled water, and dried in air at ambient temperature. The template was removed by calcination at 823 K for 6 h.

2.2. TEM, XRD, SEM Measurements. X-ray powder diffraction data of the MCM-48 molecular sieves were collected on a Seiffert TT 3000 diffractometer using Cu Kα radiation of wavelength 0.154 nm. XRD patterns were obtained between 0.5° and 10° with a scan speed of 1°/min.

Scanning electron micrographs were obtained from a Zeiss DSM 962 scanning electron microscope (Zeiss, Oberkochen, Germany). Samples were deposited on a sample holder with an adhesive carbon foil and sputtered with gold.

For specimen preparation, the samples for TEM were embedded (UHU glue, Henkel). The obtained bulks were sectioned in a Reichert Ultracut-E ultramicrotome at −55 °C (FC4E cryoattachment) set to 35 nm section thickness. The ultrathin sections were floated off the diamond knife onto a DMSO/H_2O mixture and transferred to TEM grids. Specimens were investigated in a LEO 912Ω operated at 120 kV. Elastically filtered brightfield images were recorded with a slow-scan CCD camera placed in the final image plane.

2.3. Adsorption Measurements. Adsorption and desorption isotherms were measured volumetrically on Autosorb 1-C (Quantachrome Corp., FL). Samples were outgassed at 423 K and 1×10^{-4} Torr for 13 h before measurements. Both nitrogen and argon adsorption isotherms were measured at the liquid-nitrogen temperature (77.4 K). For Ar isotherms, the saturation pressure of the supercooled-liquid Ar (230 Torr) was used.[17]

3. Adsorption Studies

Low-temperature nitrogen and argon adsorption isotherms are widely used for assessing the quality of mesoporous molecular sieves of M41S type and other nanoporous materials.[30] The shape of the isotherm is characteristic of the pore structure. In particular, for MCM-41 and MCM-48 materials, low-temperature nitrogen and argon adsorption isotherms exhibit prominent steps associated with capillary condensation in nanopores. The position of the step is determined by the characteristic pore size. The sharpness of the step is related to the pore size heterogeneity, which is expressed in terms of pore size distributions.

3.1. Limitations of Conventional Methods for Pore Size Distribution Analysis. Conventional adsorption models, which are currently used for calculations of pore structure parameters of nanoporous materials from experimental isotherms, are proven to have substantial limitations and shortcomings. The most commonly used methods for calculating the pore size distribution include the Barrett−Joyner−Halenda (BJH) and Horvath−

(9) Llewellyn, P. L.; Grillet, Y.; Schüth, F.; Reichert, H.; Unger, K. K. *Microporous Mater.* **1994**, *3*, 345.
(10) Rathouský, J.; Zukal, A.; Franke, O.; Schulz-Ekloff, G. *J. Chem. Soc. Faraday Trans.* **1995**, *91*, 937.
(11) Schmidt, R.; Stöcker, M.; Hansen, E.; Akporiaye, D.; Ellestad, O. H. *Microporous Mater.* **1995**, *3*, 443.
(12) Ravikovitch, P. I.; O Domhnaill, S. C.; Neimark, A. V.; Schüth, F.; Unger, K. K. *Langmuir* **1995**, *11*, 4765
(13) Ravikovitch, P. I.; Wei, D.; Chueh, W. T.; Haller, G. L.; Neimark, A. V. *J. Phys. Chem. B* **1997**, *101*, 3671.
(14) Kruk, M.; Jaroniec, M.; Sayari, A. *J. Phys. Chem. B* **1997**, *101*, 583.
(15) Maddox, M. W.; Olivier, J. P.; Gubbins, K. E. *Langmuir* **1997**, *13*, 1737.
(16) (a) Ravikovitch, P. I.; Haller, G. L.; Neimark, A. V. *Adv. Colloid Interface Sci.* **1998**, *76−77*, 203. (b) Ravikovitch, P. I.; Haller, G. L.; Neimark, A. V. *Stud. Surf. Sci. Catal.* **1998**, *117*, 77.
(17) Neimark, A. V.; Ravikovitch, P. I.; Grün, M.; Schüth, F.; Unger, K. K. *J. Colloid Interface Sci.* **1998**, *207*, 159.
(18) Ravikovitch, P. I.; Neimark, A. V. *Studies Surf. Sci. Catal.* **2000**, *129*, 597.
(19) Sonwane, C. G.; Bhatia, S. K.; Calos, N. *Ind. Eng. Chem. Res.* **1998**, *37*, 2271.
(20) Morishige, K.; Shikimi, M. *J. Chem. Phys.* **1998**, *108*, 7821.
(21) Floquet, N.; Coulomb, J. P.; Giorgio, S.; Grillet, Y.; Llewellyn, P. L. *Studies Surf. Sci. Catal.* **1998**, *117*, 583.
(22) Vartuli, J. C.; Schmitt, K. D.; Kresge, C. T.; Roth, W. J.; Leonowicz, M. E.; McCullen, S. B.; Hellring, S. D.; Beck, J. S.; Schlenker, J. L.; Olson, D. H.; Sheppard, E. W. *Chem. Mater.* **1994**, *6*, 2317.
(23) Schumacher, K.; Grün, M.; Unger, K. K. *Microporous Mater.* **1999**, *27*, 201.
(24) Huo, Q.; Margolese, D. I.; Ciesla, U.; Demuth, D. G.; Feng, P.; Gier, T. E.; Sieger, P.; Firouzi, A.; Chmelka, B. F.; Schüth, F.; Stucky, G. D. *Chem. Mater.* **1994**, *6*, 1176.
(25) Schumacher, K.; Du Fresne von Hohenesche, C.; Unger, K. K.; Ulrich, R.; Du Chesne, A.; Wiesner, U.; Spiess, H. W. *Adv. Mater.* **1999**, *11*, 1194.
(26) Carrazza, J.; Gonzalez, F.; Adrian, R.; Djaouadi, D.; Moore, J. G.; Shahriari, D. Y.; Landry, C. C.; Lujano, J. In *Proceedings of 12th International Zeolite Conference*; Baltimore, 1998.
(27) Zhang, S.; Fujii, Y.; Yamashita, H.; Koyano, K.; Tatsumi, T.; Anpo, M. *Chem. Lett.* **1997**, *7*, 659.
(28) Schumacher, K. Diploma thesis, Universität Mainz, 1997.
(29) Ravikovitch, P. I.; Neimark, A. V. *Langmuir* **2000**, *16*, 2419.
(30) Rouquerol, F.; Rouquerol, J.; Sing, K. S. W. *Adsorption by Powders and Porous Solids*; Academic Press: San Diego, 1999.

Kawazoe (HK) methods.[30] While these methods are incorporated in the software packages of automated commercial adsorption instruments, it has been well documented in the literature that their accuracy is limited, especially in the nanometer range of pore sizes, typical for M41S and other nanoporous materials.[6,12,13,15−18,31−32] In such confinements, the adsorbate molecules experience strong interactions with the pore walls. The Kelvin equation corrected for the multilayer adsorption on the pore walls, which is the basis of the BJH method, does not account for the adsorbate−adsorbent interactions correctly. As a result, it significantly overpredicts the pressures of the capillary condensation/desorption. Consequently, the BJH method underestimates the calculated pore size in typical MCM-41 materials by ca. 10 Å, or 25−30%.[12,13,16−18]

Recently, we have developed a new method for interpretation of adsorption isotherms and pore structure characterization of nanoporous siliceous materials.[16−18] This method is based on the NLDFT of adsorption in pores and has been implemented for nitrogen and argon adsorption in MCM-41. In previous publications, it has been shown that the NLDFT model provides a rigorous method for calculating the pore volume, specific surface area, pore size distribution, and pore wall thickness of reference MCM-41 materials[17,18] and MCM-41-based catalysts.[13,16] Below, we demonstrate the applicability of the NLDFT method to characterization of MCM-48 adsorbents.

3.2. Nonlocal Density Functional Theory Method for Pore Size Distribution Calculations. In the DFT approach,[33] the local density $\rho(\mathbf{r})$ of adsorbate confined in a pore at given chemical potential μ and temperature T is determined by minimization of the grand thermodynamic potential (GP). The GP is expressed as a functional of the local fluid density $\rho(\mathbf{r})$:

$$\Omega[\rho(\mathbf{r})] = F[\rho(\mathbf{r})] - \int d\mathbf{r}\rho(\mathbf{r})[\mu - U_{ext}(\mathbf{r})] \qquad (1)$$

where $F[\rho(\mathbf{r})]$ is the intrinsic Helmholtz free energy functional, and $U_{ext}(\mathbf{r})$ is the potential imposed by the pore walls. In a perturbation fashion, the Helmholtz free energy $F[\rho(\mathbf{r})]$ is divided into a contribution from the reference system of hard spheres, $F_{HS}[\rho(\mathbf{r})]$, and a contribution from attractive interactions, which are treated in the mean-field approximation:

$$F[\rho(\mathbf{r})] = F_{HS}[\rho(\mathbf{r})] + \frac{1}{2}\int\int d\mathbf{r}\, d\mathbf{r}'\, \rho(\mathbf{r})\rho(\mathbf{r}')\Phi_{attr}(|\mathbf{r} - \mathbf{r}'|) \qquad (2)$$

Here, $\Phi_{attr}(r)$ is the attractive potential. In this work, we use the nonlocal density functional for hard sphere fluid developed by Tarazona.[34,35] The attractive interactions are modeled by the Lennard-Jones (LJ) potential using the Weeks−Chandler−Andersen prescription.[36] Parameters of the fluid−fluid interactions (Table 1) have been chosen to reproduce the bulk thermodynamic properties of nitrogen and argon at low temperatures.[17] These include the liquid−gas coexistence densities, saturation pressure, and the surface tension of a free liquid−gas interface.

Table 1. Parameters of the Intermolecular Interactions in the NLDFT Model (refs 16−18)[a]

	fluid-fluid			solid-fluid	
adsorbate	ϵ_{ff}/k_B (K)	σ_{ff} (Å)	d_{HS} (Å)	$\rho_S\epsilon_{sf}/k_B$ (K/Å^2)	σ_{sf} (Å)
N_2	94.45	3.575	3.575	22.53	3.17
Ar	118.05	3.305	3.380	26.20	3.00

[a] ϵ_{ff}/k_B and σ_{ff} are, respectively, the well depth and the distance parameter of the Lennard-Jones potential. Fluid−fluid interactions are truncated at $5\sigma_{ff}$. d_{HS} is the diameter of hard spheres. $\rho_S\epsilon_{sf}/k_B$ and σ_{sf} are, respectively, the energetic and distance parameters of the fluid−wall interactions.

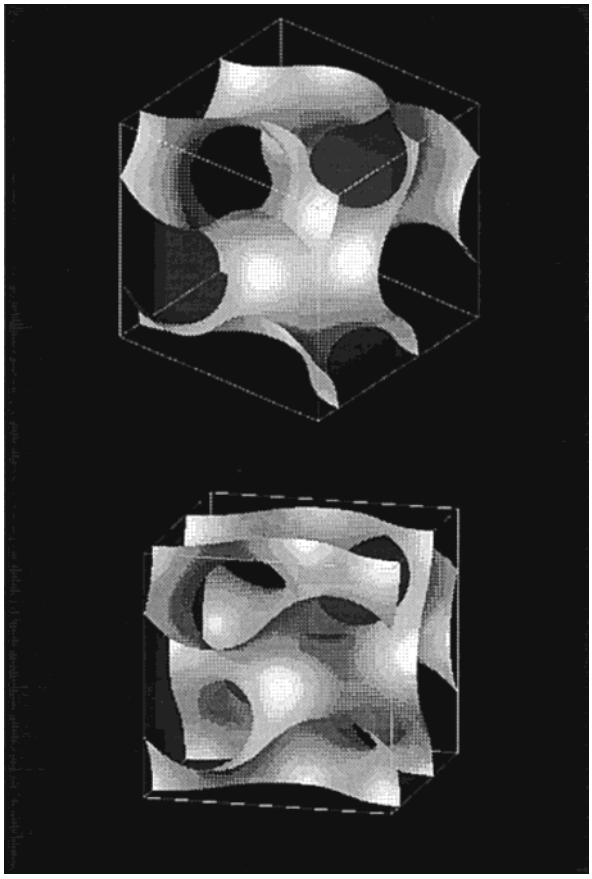

Figure 2. Minimal gyroid surface.[44]

The cylindrical pore model is used to approximate the geometry of pore channels. This approximation seems reasonable for cross sections of pores in MCM-48 (see Figure 2). The solid−fluid interactions are modeled with the LJ potential integrated over the cylindrical surface.[37] Equilibrium density profiles, $\rho(r)$, are obtained by minimization of the GP by the method of indeterminate Lagrange multipliers.[38] In the cylindrical pores, the excess adsorption per unit of pore area is expressed as

$$N_S(P/P_0) = \frac{2}{D - \sigma_{ss}}\int_0^{D/2}\rho(r)r\, dr - \frac{D - \sigma_{ss}}{4}\rho_g(P/P_0) \qquad (3)$$

Here, $\rho_g(P/P_0)$ is the bulk gas density at a given relative pressure, P/P_0; D is the pore diameter measured between the centers of the atoms in the first layer of the pore wall, and $\sigma_{ss} = 2.76$ Å is the van der Waals diameter of oxygen atom in the pore wall. Here, adsorption is defined as the excess quantity with respect to the equilibrium density

(31) Kruk, M.; Jaroniec, M.; Sayari, A. *Langmuir* **1997**, *13*, 6267.
(32) Nguyen, C.; Do, D. D. *Langmuir* **1999**, *15*, 3608.
(33) Evans, R. In *Fundamentals of Inhomogeneous Fluids*; Henderson, D., Ed.; Marcel Dekker: New York, 1992; Chapter 5.
(34) Tarazona, P. *Phys. Rev. A* **1985**, *31*, 2672; **1985**, *32*, 3148.
(35) Tarazona, P.; Marini Bettolo Marconi, U.; Evans, R. *Mol. Phys.* **1987**, *60*, 573.
(36) Weeks, J. D.; Chandler, D.; Andersen, H. C. *J. Chem. Phys.* **1971**, *54*, 5237.
(37) Tjatjopoulos, G. J.; Feke, D. L.; Mann, J. A., Jr. *J. Phys. Chem.* **1988**, *92*, 4006.
(38) Neimark, A. V. *Langmuir* **1995**, *11*, 4183.

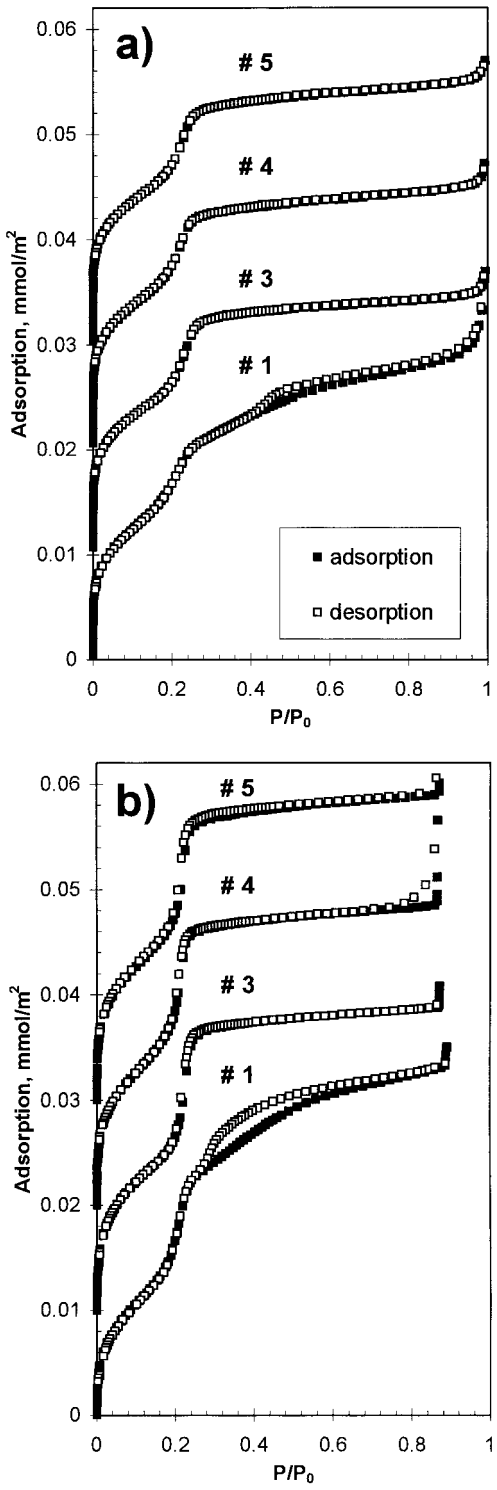

Figure 3. Nitrogen (a) and argon (b) adsorption and desorption isotherms at 77 K on MCM-48 materials. Isotherms are normalized by surface areas obtained by the comparison method using the isotherm on reference MCM-41 material. For samples 3, 4, and 5, the scale is shifted by 0.01, 0.02, and 0.03 mmol/m^2, respectively.

in the bulk, and the reference fluid volume is defined as the internal volume of the cylindrical pore of diameter $D_{in} = D - \sigma_{ss}$. Parameters of the solid−fluid interactions (Table 1) have been obtained to reproduce the standard nitrogen and argon isotherms on nonporous oxides.[16−18]

To quantify the pore size heterogeneity in terms of a pore size distribution, the experimental isotherm is represented as a combination of theoretical isotherms in individual pores:

$$N_{exp}(P/P_0) = \int_{D_{min}}^{D_{max}} \varphi_S(D_{in}) N_S(D_{in}, P/P_0)\, dD_{in} \quad (4)$$

where $N_S(D_{in},P/P_0)$ is the theoretical adsorption in a pore of size D_{in}, $\varphi_S(D_{in})$ is the pore size distribution. Unlike the BJH method, eq 4 also accounts for variations of the adsorbate density in filled pores, which is somewhat greater than the bulk−liquid density. It should be noted that the networking effects caused by intersections of pores of different sizes[39] are not considered in this approach. Despite the regular cubic network formed by MCM-48 pore channels, the absence of absorption hysteresis (see Figure 3) and the uniform pore size distributions (see Figure 4) imply that the networking effects should not be significant.

To calculate the pore size distribution, the integral eq 4 is inverted using the discrete Tikhonov regularization method, which minimizes the 2-norm of the solution vector.[40,41] When constructing the kernel of the integral eq 4, we took advantage of the well-established experimental observation that the experimental isotherms on mesoporous molecular sieves of MCM-41 and MCM-48 type reduced per unit of pore area are similar in the mono- and multilayer adsorption region.[8,12,13,16,42] Therefore, to represent the kernel isotherms in this region of relative pressures, we used the reference isotherm on well-characterized wide-pore MCM-41 material.[12,17] This procedure simplifies the solution of the eq 4 and does not affect the calculated pore size.

3.3. Calculation of Pore Wall Thickness in MCM-48 from Adsorption and X-ray Diffraction. Recently, a systematic approach to structural characterization of templated nanoporous materials with cubic symmetry by gas adsorption isotherms has been proposed.[29] The approach implies that a solid skeleton of the porous material retains the symmetry and topology of the mesophase system used as a template during the synthesis. When the parental mesophase forms a bicontinuous periodic structure, which can be described as a triply periodic minimal surface (TPMS),[2,43,44] the solid phase in the templated porous matrix is bounded by surfaces located at an equal distance from the central TPMS.

In mathematical terms, the TPMS is a surface of zero mean curvature, $H = (1/2)(1/R_1 + 1/R_2) = 0$, and negative Gaussian curvature, $K = 1/(R_1R_2)$; here, R_1 and R_2 are the local principal radii of curvature. Thus, on the minimal surface, $R_1 = -R_2$ in each point, and the surface is saddle shaped everywhere. The Gauss−Bonnett theorem[43,44]

$$\int_A K\, dA = \langle K \rangle A_{UC} = 2\pi\chi \quad (5)$$

relates the mean Gaussian curvature, $\langle K \rangle$, averaged over the surface, the surface area per unit cell of the periodic structure, A_{UC}, and the Euler−Poincaré parameter, $\chi = \langle K \rangle A_{UC}/2\pi$.

When dealing with cubic symmetries, it is convenient to use the dimensionless quantities reduced per length of

(39) Neimark, A. V. *Stud. Surf. Sci. Catal.* **1991**, *62*, 67.
(40) Lawson, C. L.; Hanson, R. J. *Solving Least Squares Problems*, SIAM: Philadelphia, 1995.
(41) Hansen, P. C. *Numer. Algorithms* **1994**, *6*, 1.
(42) Kruk, M.; Jaroniec, M.; Ryoo, R.; Kim, J. M. *Chem. Mater.* **1999**, *11*, 2568.
(43) Andersson, S.; Hyde, S. T.; Larsson, K.; Lidin, S. *Chem. Rev.* **1988**, *88*, 221.
(44) Góźdź, W.; Hołyst, R. *Periodic Surfaces in Physics, Chemistry and Biology*; Encyclopedia of Applied Physics, Wiley Verlag: New York, 1999.

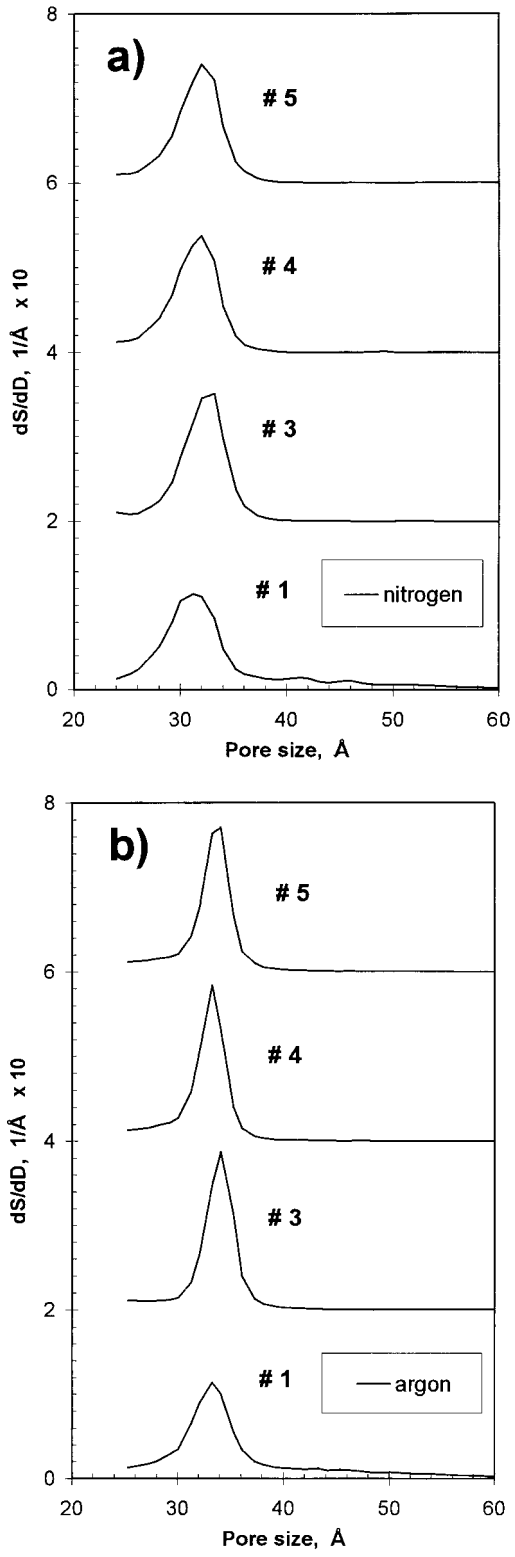

Figure 4. Pore size distributions of MCM-48 materials calculated by the NLDFT method from nitrogen (a) and argon (b) adsorption isotherms. The scale is shifted for convenience.

the crystallographic unit cell, a, which can be obtained from the XRD pattern:

$$a = \mathrm{d}_{hkl}\sqrt{h^2 + k^2 + l^2} \tag{6}$$

In so doing, the dimensionless area per unit cell of periodic surface is defined as $\xi_0 = A_{UC}/a^2$. The Euler−Poincaré parameter, χ, and reduced area of the unit cell, ξ_0, are determined by the symmetry of the structure, which can be determined by the XRD. The scaling factor, the length of the unit cell, a, is determined from the XRD patterns and TEM pictures.

For MCM-48, which has been described as the bicontinuous structure centered on the gyroid minimal surface,[3,4] the reduced area per crystallographic unit cell is equal to $\xi_0 = 3.092$.[2] The image of the gyroid minimal surface is presented in Figure 2. The cubic network of pores with nearly circular cross section is clearly seen.

When the Euler−Poincaré parameter, $\chi = \langle K \rangle A_{UC}/2\pi$, is small, the geometrical parameters of a templated porous structure fulfill the following equations.[29] The porosity, ϵ, or the fraction of pores in the unit cell, is related to the mean pore wall thickness, $\langle h \rangle$, as

$$\epsilon = 1 - \xi_0(\langle h \rangle/a) \tag{7}$$

Introducing the hydraulic pore diameter, D_h

$$D_h = a(2\epsilon/\xi_0) \tag{8}$$

the pore wall thickness and the hydraulic pore diameter are related as

$$a/\xi_0 = \langle h \rangle + D_h/2 \tag{9}$$

The geometrical parameters featuring in eqs 7−9 are directly related to the parameters calculated from the gas adsorption isotherms: the specific surface area, pore volume, and pore size distribution. From the adsorption measurements, one obtains the parameters per unit mass, i.e., the pore volume V_P (cm^3/g), and specific surface area, S (m^2/g). By use of the true density of solid, ρ_S (g/cm^3), which can be obtained from helium pycnometry, the porosity is expressed as

$$\epsilon = \frac{\rho_S V_P}{1 + \rho_S V_P} \tag{10}$$

The reduced area of the unit cell is related to the specific surface area as

$$\xi_0 = (1 - \epsilon)\rho_S a\left(\frac{S}{2}\right) \tag{11}$$

The hydraulic pore diameter, D_h, is unambiguously determined by the pressure of the capillary condensation step and, therefore, can be taken from the pore size distribution, for example, as the mean pore size. In the previous publication, it has been shown that the NLDFT method gives very accurate estimates of the mean pore diameters in reference MCM-48 materials.[29]

Equation 9 has an advantage of being independent of any absolute quantity (per unit weight), which may be inaccurate due to uncontrolled impurities in the sample or inaccuracies in the weight measurements. Note that although the true density of silica-based templated materials is usually taken equal to the amorphous silica density ($\rho_S = 2.2$ g/cm^3), strikingly different values were reported in the literature.[15,19,21] Therefore, eq 9, which involves only the unit cell length, a, and the pore diameter, D_h, is the preferred way for calculating the pore wall thickness (Table 2). Both these parameters are reliably determined, the first from the XRD pattern and the second from the adsorption isotherm. In the case of the isotherms with prominent step (similar to those reported in Figure 4), the characteristic pore diameter of MCM-48 can be obtained with reasonable accuracy from the inflection

Table 2. Pore Structure Parameters of MCM-48 Materials Calculated from XRD and Adsorption Data[a]

		nitrogen				argon	
sample	a, Å	S_{meso}, m^2/g	V_{meso}, cm^3/g	D_h, Å	$\langle h \rangle$, Å	D_h, Å	$\langle h \rangle$, Å
1	78.7	660	0.53	31	9.9	33	9.0
2	79.7	970	0.74	33	9.3		
3	79.5	1010	0.80	33	9.2	34	8.7
4	75.8	830	0.64	32	8.5	33	8.0
5	77.8	830	0.66	32	9.2	33	8.7

[a] $a = d_{hkl}(h^2 + k^2 + l^2)^{1/2}$ is a cubic lattice parameter calculated from XRD. S_{meso} is the specific surface area obtained from the comparison plot. V_{meso} is the specific pore volume estimated from the plateau on the isotherm after the step. D_h is the mean pore diameter calculated from the NLDFT pore size distribution. $\langle h \rangle$ is the mean pore wall thickness calculated from sorption and XRD data using eq 9.

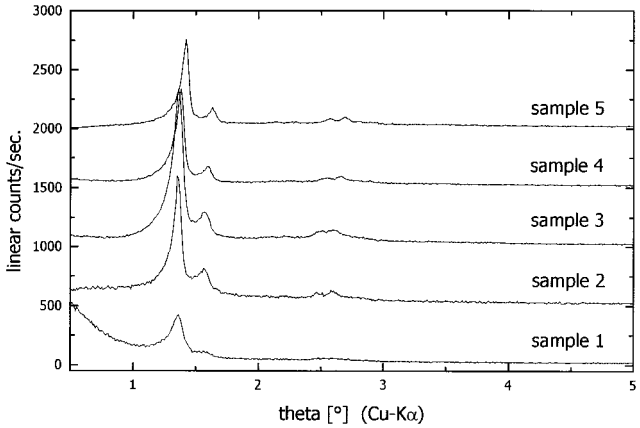

Figure 5. XRD of the MCM-48 samples.

point of the isotherm using the NLDFT pore size-filling pressure dependence.[16a,18]

4. Results and Discussion

X-ray diffractograms of MCM-48 produced by the hydrothermal (sample 2) and by the room temperature reaction (samples 3−5) (Figure 5) are identical to the one reported by Mobil researchers.[1,22] Uncalcined MCM-48 shows a broader 211 interference than calcined material (data not shown). All the samples prepared by the room temperature method exhibit five peaks, which could be indexed to the space group $Ia3d$. The samples prepared by the hydrothermal method differ in the quality of the material. Sample 2, which has been synthesized for 10 days, shows five peaks, while sample 1 shows only 3. The lack of quality of sample 1 is due to the short reaction time.

Scanning electron images of MCM-48 samples prepared by the hydrothermal synthesis and the room temperature synthesis are shown in Figure 6.Nonagglomerated uniform spheres were obtained by the room temperature method while irregularly shaped particles where obtained by the hydrothermal synthesis. The spherical particle morphology is presumably due to the presence of ammonia, which is known as a morphology catalyst,[45] but the reaction mechanism is not fully understood.

Transmission electron micrographs provide visualization of the pore structure. Thin sections of calcined MCM-48 are shown in Figure 7. A part of a spherical particle is shown on the micrograph in Figure 7a. The pore structure is regular over the whole particle. Figure 7b

(45) Iler, R. K. *The Chemistry of Silica*; Wiley: New York, 1979.

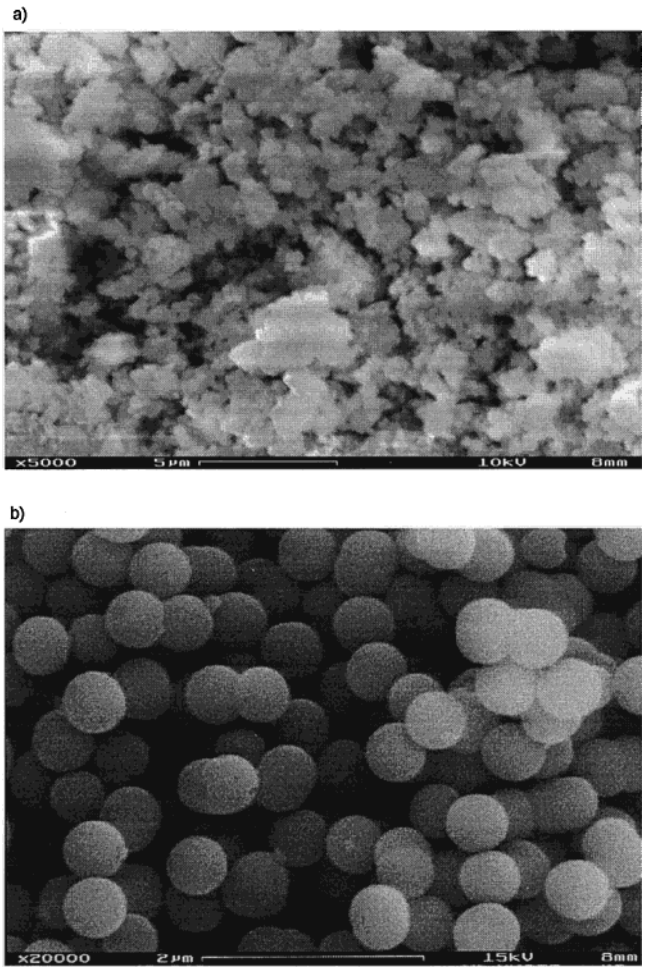

Figure 6. SEM of the MCM-48 samples prepared by the hydrothermal (a) and room temperature (b) syntheses.

shows the pore structure along the cubic [110] plane. The TEM picture allows one to estimate the pore size (∼30 Å) and the pore wall thickness (∼10 Å).

Adsorption isotherms of nitrogen and argon at 77 K are shown in parts a and b, respectively, of Figure 3. The isotherms have been reduced on the surface areas obtained by the comparison method using the reference well-characterized wide-pore MCM-41 material.[12,17] The isotherms exhibit sharp steps in the relative pressure range $P/P_0 = 0.2-0.3$, which are associated with capillary condensation in channels of MCM-48 structure. No hysteresis is observed. The sharpness of the capillary condensation steps indicates uniformity of pore channels and their narrow size distribution. For such type of isotherms networking effects should not be significant. We note that for argon, these steps are more vertical and shifted to smaller relative pressures. This is consistent with the lower reduced temperature (T/T_c, where T_c is the bulk critical temperature) of Ar at 77 K as compared to N_2 at 77 K, and with the smaller size of the Ar molecule.[13,17] The adsorption isotherms on sample 1 exhibit also filling of a secondary pore structure as manifested by the increase in adsorption at the relative pressures $P/P_0 = 0.3-0.6$ accompanied by hysteresis loop. This behavior indicates lower quality of the sample prepared using short reaction times and is consistent with the XRD pattern (Figure 5).

Pore size distributions have been calculated by the NLDFT method described above (Figure 4). For all the materials studied, the mean pore diameter is approximately 31−33 Å with a standard deviation of ca. 1−2 Å.

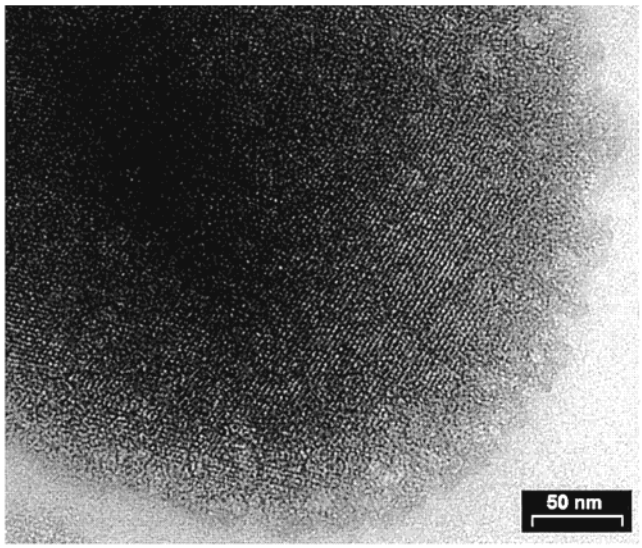

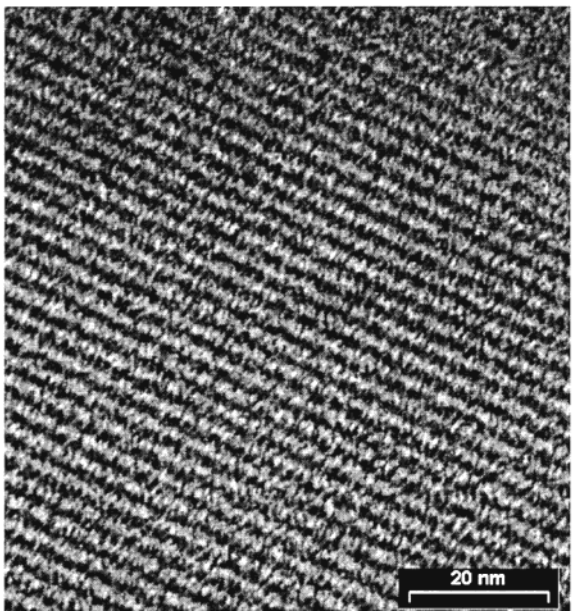

Figure 7. TEM of MCM-48 spherical particle prepared by the room temperature synthesis (a); view along the cubic [110] plane (b).

We note a satisfactory agreement between the pore size distributions obtained from nitrogen and argon adsorption isotherms.

To calculate the mean pore wall thickness from the capillary condensation data and X-ray diffraction by the method described above, we substituted the mean pore diameters obtained from the pore size distributions into eq 9 and used $\xi_0 = 3.092$ for the dimensionless area of the minimal gyroid surface.[2] The calculated wall thicknesses are presented in Figure 8. The results are plotted as a function of the unit cell length. The pore wall thickness

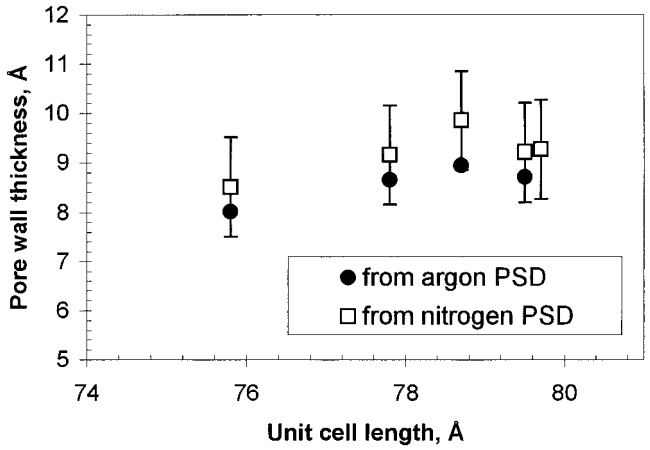

Figure 8. Pore wall thickness of MCM-48 calculated from XRD and capillary condensation data.

of MCM-48 materials lies in the interval from ca. 8 to 10 Å (Table 2). This is comparable with the estimates obtained from TEM (Figure 7b) and with the wall thickness of hexagonal MCM-41 materials of similar pore size.[16b,17]

5. Conclusions

MCM-48 materials have been prepared at different conditions and studied by TEM, XRD, SEM, and low-temperature nitrogen and argon adsorption. It has been demonstrated that the novel room temperature synthesis yields highly ordered MCM-48 materials. Moreover, nonagglomerated uniform spheres of size ca. 0.5 μm have been obtained.

It has been shown that the NLDFT-based approach provides rigorous method for interpreting the adsorption isotherms and calculating the pore structure parameters of MCM-48 type adsorbents. The pore size distributions calculated independently from the nitrogen and argon isotherms are in satisfactory agreement.

A novel approach to calculating the pore wall thickness of MCM-48 from XRD and gas adsorption isotherms has been employed. The approach utilizes intrinsic symmetry of MCM-48 pore structure revealed by XRD and combines the results of the pore size distribution analysis with general geometrical relations between structural parameters of the gyroid minimal surface. The pore wall thickness of MCM-48 is found to be ca. 8−10 Å.

Acknowledgment. This work was supported, in part, by the Bundesministerium für Bildung, Wissenschaft, Forschung und Technologie (BMBF No. 03D0068B5), the TRI/Princeton exploratory research program, and the Alexander von Humbolt Foundation. The authors thank Merck KGaA for supplying chemicals, Quantachrome Corp. for a free loan of adsorption instrument, and W. Góźdź and R. Hołyst for permission to reproduce the computer images of the gyroid surface.

LA991595I